The Role of Acoustic Streaming in Ultrasound-Enhanced Electrospinning - a FEM Simulation Study

Mäkinen, Joni Mikko Kristian

IEEE
2022

Mäkinen , J M K , Schavikin , J , Österberg , H O , Valoppi , F , Nikolaev , D , Laidmäe , I , Heinämäki , J , Salmi , A & Haeggström , E 2022 , The Role of Acoustic Streaming in Ultrasound-Enhanced Electrospinning - a FEM Simulation Study . in 2022 IEEE International Ultrasonics Symposium (IUS) . IEEE , 2022 IEEE International Ultrasonics Symposium (IUS) , Venice , Italy , 10/10/2022 . https://doi.org/10.1109/IUS54386.2022.9957535

http://hdl.handle.net/10138/354503
https://doi.org/10.1109/IUS54386.2022.9957535

submittedVersion

The Role of Acoustic Streaming in Ultrasound-Enhanced Electrospinning – a FEM Simulation Study

Joni Mäkinen*, Johannes Schavikin*, Henri Österberg*, Fabio Valoppi*†‡, Dmitry Nikolaev*,
Ivo Laidmäe§, Jyrki Heinämäki§, Ari Salmi* and Edward Hæggström*
*Electronics Research Lab., Dept. of Physics, University of Helsinki, Finland
†Dept. of Food and Nutrition, University of Helsinki, Finland
‡Helsinki Institute of Sustainability Science, Faculty of Agriculture and Forestry, University of Helsinki, Finland
§Institute of Pharmacy, University of Tartu, Estonia
Email: joni.mk.makinen@helsinki.fi

***Abstract*—We present a finite element method (FEM)-based simulation model for acoustic streaming and fountain formation. Streaming field predicted by the model shows agreement with experiments in a validation study. After validation, the model is used to predict the acoustic streaming field in our ultrasound-enhanced electrospinning device. The predicted field gives velocity magnitudes in the micrometers per second range. While this appears slow, such a rate is hypothesized to be significant for the process. Finally, surface force driven acoustic streaming is observed by the simulations.**

***Index Terms*—Electrospinning, Acoustic streaming, Acoustic fountain, FEM, Nonlinear acoustics**

I. Introduction

Nonlinear acoustic phenomena find many practical applications, and several modeling approaches exist in the literature. For example, acoustic drop sampling to transport small semiconductor chips has been shown and modeled using the finite element method (FEM) where surface forces deform and break a liquid-air boundary [1]. Acoustic streaming also finds many applications and it has been modeled using FEM for, e.g., microchannel applications [2].

Our interest is FEM modeling of our ultrasound-enhanced electrospinning (USES) device [3]. In USES, focused ultrasound impinges on a polymer-solution-air interface creating an acoustic fountain. When a high-voltage is applied between the solution and a collector plate, the solution jets from the fountain starting the electrospinning process. In electrospinning, the polymer solution is drawn by the high-voltage electric field such that nano- to micrometer caliber fibers are formed.

Here we continue our modeling work on USES. Previously, we presented a FEM study on the formation of the acoustic fountain [4]. Now we predict the acoustic streaming inside the polymer solution. Different ultrasound driving parameters affect the produced fibers' diameter in USES [5] and as such, we expect that acoustic streaming could be one of the phenomena related to this.

II. Theory

To model the streaming field, we use the standard perturbation approach starting from the Navier-Stokes equations. The same approach was used in [2] with FEM for flows in microchannels.

We model the fluid dynamics with the Navier-Stokes equations in their conservative form together with the continuity equation:

$$\partial_t(\rho\vec{u}) + \nabla\cdot(\rho\vec{u}\otimes\vec{u}) = -\nabla p + \nabla\cdot\boldsymbol{\sigma} + \rho\vec{g} \tag{1}$$

$$\boldsymbol{\sigma} = \mu\left(\nabla\vec{u} + (\nabla\vec{u})^T - \frac{2}{3}(\nabla\cdot\vec{u})\boldsymbol{I}\right) + \mu_B(\nabla\cdot\vec{u})\boldsymbol{I}$$

$$\partial_t\rho + \nabla\cdot(\rho\vec{u}) = 0 \tag{2}$$

Here we have density ρ, velocity $\vec{u}$, pressure p, gravitational acceleration $\vec{g}$, dynamic viscosity μ, bulk viscosity μ_B and $\boldsymbol{I}$ is the identity tensor.

To simplify the model, temperature of the system is not included in this study, and the standard equation of state is used to link pressure and density together:

$$p = c_0^2\rho, \tag{3}$$

where c_0 is the speed of sound.

The perturbation is carried up to the second order:

$$p = p_0 + p_1 + p_2$$
$$\vec{u} = 0 + \vec{u}_1 + \vec{u}_2$$
$$\rho = \rho_0 + \rho_1 + 0$$

Here the zeroth-order perturbation is the equilibrium, with quiescent background flow. p_0 and ρ_0 are the ambient pressure and density respectively. The first-order perturbation is the linear acoustic field while the second-order perturbation gives then the acoustic streaming field. The density is only accounted for up to the first order, as is standard, while the higher-order terms would be associated with the generation of higher harmonics.

Applying this perturbation in the first order and assuming a time-harmonic solution ($e^{i\omega t}$ convention) to (1) and (2) while using (3) leads to the following equations for the acoustic field:

$$i\omega\rho_0\vec{u}_1 = \nabla\boldsymbol{\sigma}_1 \tag{4}$$

$$\frac{i\omega}{c_0^2}p_1 + \rho_0\nabla\cdot\vec{u}_1 = 0 \tag{5}$$

In the second order, when we make use of the fact that the acoustic time scale is much shorter than that of the streaming field, we get:

$$\rho_0\partial_t\vec{u}_2 = \nabla\cdot\boldsymbol{\sigma}_2 + \rho_0\vec{g} - \langle 2i\omega p_1\vec{u}_1\rangle - \nabla\cdot\langle\rho_0\vec{u}_1\otimes\vec{u}_1\rangle \tag{6}$$

$$\nabla\cdot\langle\rho_1\vec{u}_1\rangle + \rho_0\nabla\cdot\vec{u}_2 = 0 \tag{7}$$

Time-averaging ($\langle\cdot\rangle$) over the acoustic period removes the linear first-order terms while retaining any terms related to nonlinearity. Here we can see that in (6) we have the Stokes equations with added acoustic volume force terms on the right-hand-side. These forces drive the acoustic streaming.

The reason for using the conservative form in (1) is the divergence form for the nonlinearity of the velocity field on the left-hand-side. This leads to a force term of the same form ($-\nabla\cdot\langle\rho_0\vec{u}_1\otimes\vec{u}_1\rangle$) in the streaming equations (6) from the first-order fields (4). From this, we can extract the following surface force which can also induce streaming together with the volumetric forces:

$$\vec{F}_s = \vec{n}\cdot\langle\rho_0\vec{u}_1\otimes\vec{u}_1\rangle, \tag{8}$$

where $\vec{n}$ is the surface normal vector. Full derivations for these equations can be found from [6].

Since USES employs polymer solutions, which are non-Newtonian liquids, we need to consider the dynamic viscosity μ in the equations. For now, we have assumed that this viscosity can be split into its zero shear-rate value μ_0 and its infinite shear-rate value μ_∞. With this split, we assume that it is sufficient to start by modeling the acoustic field (4), (5) using $\mu = \mu_\infty$ and the streaming field (6), (7) using $\mu = \mu_0$.

III. Methods

The main objective of this study was to build a FEM simulation to predict acoustic streaming in USES. For that, we chose aqueous poly(ethylene oxide) (PEO) ($M_v \sim 900000$, Sigma-Aldrich, Missouri, USA) solution, 4 wt%, as our test liquid. We also wanted to validate the simulation model for the acoustic streaming. For that, optical methods (Section III B.) were chosen. We needed to change the opaque PEO solution to a translucent liquid, for which we chose vegetable oil (Keiju Rypsiöljy, Bunge Finland Oy, Raisio, Finland).

A. Simulations

The FEM model was built using COMSOL Multiphysics® v6.0 (COMSOL AB, Stockholm, Sweden). Fig. 1 a) shows the axisymmetric geometry of the USES model. The device features two domains: 1) the polymer solution container and 2) a water chamber that hosts the focusing transducer. The transducer operates at $f = 2.7\,\mathrm{MHz}$ and the dimensions are

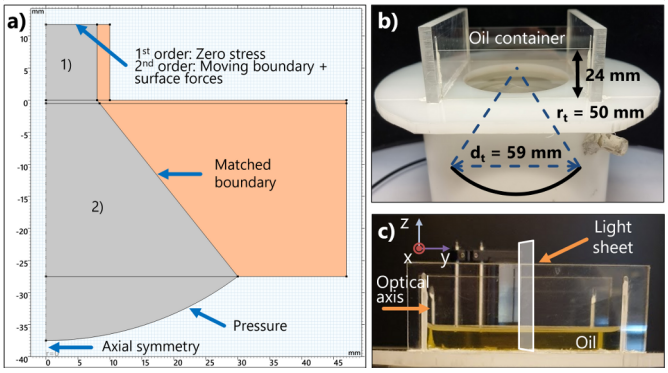

Fig. 1. a) Simulation geometry of USES. Orange area was neglected in the simulations, main boundary conditions are indicated. Domain 2) is water and domain 1) is PEO solution or oil. When oil was used, domain 1) was extended in the radial direction to better match the geometry in b). b) Modified USES set-up for validation with a larger container for oil. The focusing transducer ($r_t = 50\,\mathrm{mm}$ and $d_t = 59\,\mathrm{mm}$) is illustrated in the picture. c) Side-view of the oil container in b) showing the direction of the optical axis, oil, and the light-sheet. xz-plane corresponds to the symmetry plane of the simulation.

shown in Fig. 1. For validation simulations, domain 1) was extended in the radial direction. The whole USES geometry is shown, but only the gray part was considered to speed up the simulations. In Fig. 1, domain 1) is of most interest, here the acoustic field (4), (5) was solved using COMSOL's built in *Thermoviscous Acoustics* equations. The streaming field (6), (7) was also solved here, using COMSOL's *Creeping Flow* equations to solve for the Stokes flow. The nonlinear terms from the first-order fields were added manually using weak-form expressions. Our model also solves for the formation of the acoustic fountain. This was accomplished with COMSOL's *Moving Mesh*. A *Free Surface* boundary condition (BC) was applied on the top boundary which defines the force balance on the surface in the Stokes equations together with surface tension (σ_{st}). To apply the surface force from the acoustic field (8), a boundary weak-form contribution was manually added to the equations.

For the acoustic field in domain 1), the top surface was set as a no-stress BC ($\vec{n}\cdot\boldsymbol{\sigma}_1 = 0$). In domain 2), streaming was not solved for, and the acoustic field was solved using the standard wave equation (*Pressure Acoustics* in COMSOL) to reduce the size of the simulation. To ignore the region shown in orange (Fig. 1 a)), the boundary was set as an impedance matched boundary to allow the acoustic energy to exit the system. The transducer was modeled with a pressure BC ($p_1 = 3.5\,\mathrm{kPa}$ for validation with oil, $p_1 = 23\,\mathrm{kPa}$ for PEO) based on previous simulations and experiments of the streaming field [6].

The following material parameters were used in the simulations: PEO solution: $c_0 = 1519\,\mathrm{m/s}$ [4], $\rho_0 = 1000\,\mathrm{kg/m^3}$ [4], $\mu_0 = 7.1\,\mathrm{Pa\cdot s}$ [7], $\mu_\infty = 0.03\,\mathrm{Pa\cdot s}$ [7] and $\sigma_{st} = 62\,\mathrm{mN/m}$ [8]. Vegetable oil: $c_0 = 1455\,\mathrm{m/s}$ [9], $\rho_0 = 914.5\,\mathrm{kg/m^3}$ [10], $\mu = 67.8\times10^{-3}\,\mathrm{Pa\cdot s}$ [10] and $\sigma_{st} = 33.8\,\mathrm{mN/m}$ [11]. The bulk viscosity μ_B was assumed to be equal to the dynamic viscosity μ. Water parameters were obtained from COMSOL's material library.

The simulations were run in time domain for the second-order fields together with the moving mesh. The acoustic field was computed in the frequency domain at each time step in the deformed mesh.

B. Measurements and analysis

Fig. 1 shows the modified USES set-up with vegetable oil that we employed in the validation measurements. The height of the oil was varied to obtain different streaming results.

The imaging was done with a stroboscopic schlieren setup [12] coupled with a custom white light LED light-sheet, approximate width of $4\,\mathrm{mm}$, for particle imaging (PI). Schlieren imaging was used to assess the acoustic field shape, and PI was used to gather data for particle imaging velocimetry (PIV) to measure the acoustic streaming field. Silica microspheres (mean diameter $14.2\,\mu\mathrm{m}$, Osaka Soda CO., LTD., Osaka, Japan) were used for PI.

The transducer was driven with a continuous wave at $f = 2.7\,\mathrm{MHz}$ with fixed amplitude. The signal was generated with a signal generator (AFG31052, Tektronix, inc., Oregon, USA) and was amplified with an RF amplifier (BT00100-AlphaA-CW, Tomco Technologies, South Australia, Australia). Voltage amplitude at the transducer, $2.2\,\mathrm{V}$, was measured with an oscilloscope (PicoScope 2204A, Pico Techonology, Cambridgeshire, United Kingdom). The stroboscopic schlieren was operated and synced with the same signal generator. Image-acquisition was done with a camera (UI-3480CP, IDS Imaging Development Systems GmbH, Obersulm, Germany) connected to a PC.

Data was plotted with MATLAB R2021a (The MathWorks, Inc., Massachusetts, USA) and the PIV analysis was conducted with PIVlab [13]. The experimental data shown here was measured for [6], and re-analyzed here.

IV. Results

Fig. 2 shows the results of the validation using vegetable oil. Two cases of initial oil surface placement are shown. First, the oil is set above the geometric focal plane of the transducer leading to an upwards streaming field. In the second configuration, the oil surface is set below the focal plane such that the streaming reverses direction as the acoustic field focuses below the surface, after reflecting from it. Here the experimental result shows a broken symmetry due to a slight tilt in the system, though still showing a tendency to flow downward like in the simulation. The schlieren images also show that the acoustic focal spot is where we expect it to be. The schlieren images are not exactly comparable to the simulations as schlieren also integrates refractive index changes through the optical axis. Blurriness in the schlieren images is due to the microspheres. Fig. 2 d) shows that due to the glass wetting from the oil we couldn't see the acoustic fountain and thus couldn't compare this to the simulations.

Fig. 3 shows the simulation predictions for the PEO solution. Again, two surface configurations w.r.t. the focal plane were chosen. Depending on the choice, the acoustic fountain is either sharp when near the focus in a), or flat when far away from the focus in b). The streaming field changes direction near the surface in b). The case in a) reflects the configuration we would use in USES operation. The predicted flow in the streaming field is low, in the micrometers per second range. In b) a region of downwards pointing streaming is localized near the surface.

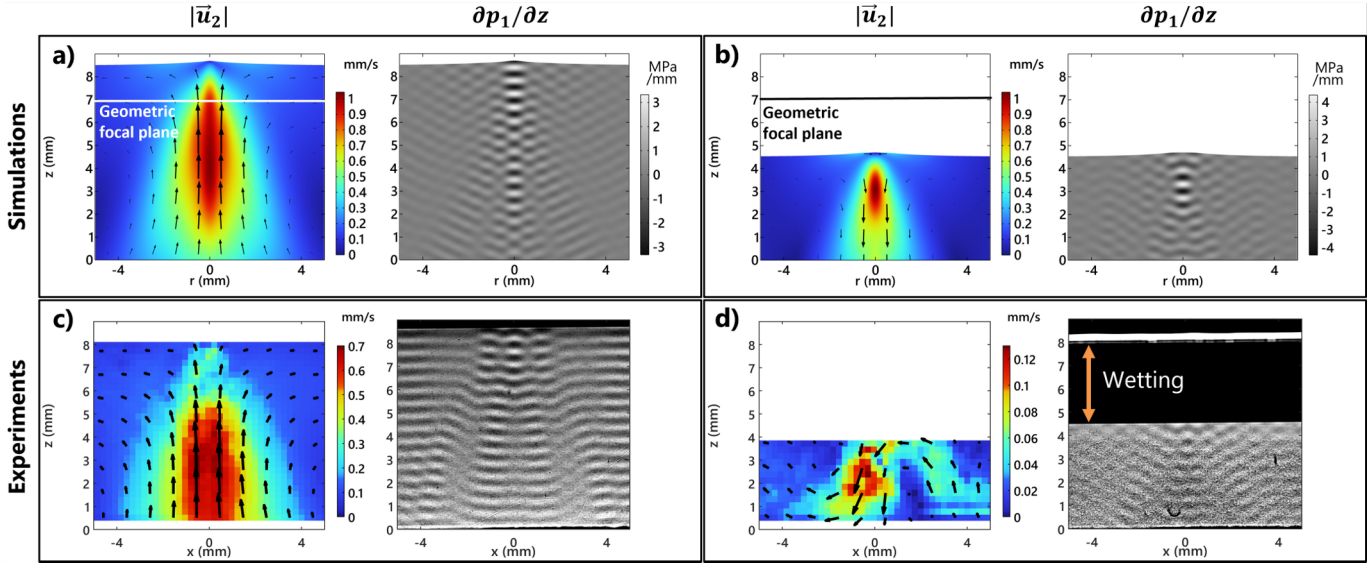

Fig. 2. Simulated and measured acoustic and streaming fields in two surface level configurations. a) and b): Simulation results for the oil surface above and below the geometric focal plane, respectively. c) and d): corresponding experimental results (PIV for the velocity and schlieren for the acoustic field). Velocity magnitude and vectors are plotted for the streaming field. The schlieren system measures the z-directional derivative of the refractive index ($\propto \rho_1 \propto p_1$). To compare with the simulations, the z-directional derivative of the instantaneous pressure (p_1) is plotted. Wetting of the glass surface is also indicated in d). In d) the flow field makes an s-shaped pattern due to a tilt in the measurement system.

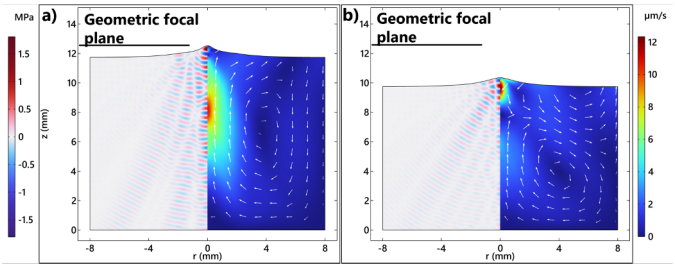

Fig. 3. Simulation prediction for acoustic streaming in USES with 4 wt% aqueous PEO solution. a) Surface set to slightly below the geometric focal plane of the transducer and the streaming points upwards. In b) the surface is set to significantly below the focal plane and the streaming points downwards near the surface.

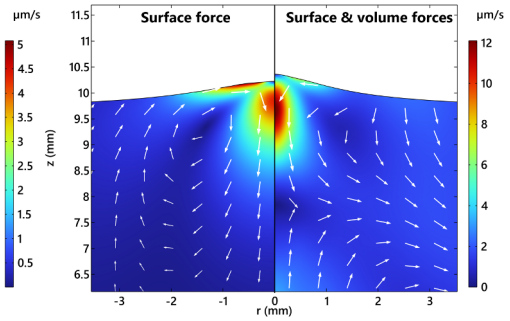

Fig. 4. Simulation prediction of surface-force-induced streaming. On the right: the same result as in Fig. 3 b) but zoomed in. On the left: the same configuration but without the volumetric forces, only the surface force (8). This shows that a significant streaming can be attributed to surface forces.

This led to the final simulation where we investigated this surface streaming pattern. Fig. 4 shows a comparison of the configuration in Fig. 3 b) with a simulation using just the surface force (8), which includes only the velocity term. Notice the difference in the fountain height, which is the result of neglecting the volume force terms, namely the term with both pressure and velocity as the pressure is not exactly zero at the surface in the zero-stress BC approximation we used here.

V. Discussion

Fig. 2 showed agreement in the flow patterns between the simulation predictions and the experimental measurements. The discrepancy in b) vs d) is caused by tilt in the experimental system, which broke the streaming symmetry. The result is interesting in its own right for USES. If acoustic streaming is important, the tilt of the system needs to, depending on the flow pattern, be precisely controlled.

One way to affect the fiber diameter in traditional electrospinning is to increase the polymer solution feed rate [14]. In USES, the equivalent process is a combination of the acoustic streaming and the surface forces, which generate the acoustic fountain. In USES operation, polymer solution is consumed at $\sim 1\,\mathrm{ml/h}$. The acoustic fountain is $2\,\mathrm{mm}$ wide, so if we were to produce the same flow rate with streaming through the fountain, the velocity needs to be $u = (1\,\mathrm{ml/h})/(\pi(1\,\mathrm{mm})^2) \approx 90\,\mu\mathrm{m/s}$. The results in Fig. 3 a) show that the streaming upwards through such a cylinder is in the order of 10 μm/s, meaning that the streaming velocity is significant compared to the solution consumption rate. This result supports the hypothesis that streaming could play a key role in USES, but a more complete simulation model with the fiber drawing process included would be needed to draw strong conclusions. The simulation makes significant assumptions about the viscoelasticity of the PEO solution, which also needs further considerations.

As a side product of the USES simulations, we observed a surface force driven flow in the simulations (Fig. 4). This surface streaming requires the equations to be formulated such that the acoustic velocity is solved as an independent variable. Consequently, the force expression on the surface (8) can have a tangential component giving rise to such a flow.

VI. Conclusions

We presented a FEM-based simulation model for USES, which accounts for acoustic fountain formation together with acoustic streaming. The model also predicted surface force driven streaming. The simulated flow patterns showed similarity with the experimental results. A slow - yet significant - streaming field was predicted for USES.

References

[1] Y. Tang and E. S. Kim, "Nozzleless acoustic droplet ejector with electrically tunable droplet size for picking and placing semiconductor chips," *J. Microelectromech. S.*, vol. 30, no. 2, pp. 262–270, Apr. 2021.

[2] P. B. Muller and H. Bruus, "Numerical study of thermoviscous effects in ultrasound-induced acoustic streaming in microchannels," *Phys. Rev. E*, vol. 90, no. 4, p. 043016, Oct. 2014.

[3] H. J. Nieminen *et al.*, "Ultrasound-enhanced electrospinning," *Sci. Rep.*, vol. 8, no. 1, p. 4437, Mar. 2018.

[4] J. Mäkinen *et al.*, "FEM modelling of ultrasound enhanced electrospinning (USES)," in *2019 IEEE IUS*, Oct. 2019, pp. 2511–2514.

[5] E. Hakkarainen *et al.*, "Comparison of traditional and ultrasound-enhanced electrospinning in fabricating nanofibrous drug delivery systems," *Pharmaceutics*, vol. 11, no. 10, p. 495, Oct. 2019.

[6] J. Mäkinen, "FEM model of acoustic streaming and the fluid-air interface deformation due to acoustic and electric forces in ultrasound-enhanced electrospinning," Master's thesis, University of Helsinki, Helsinki, 2022.

[7] K. W. Ebagninin, A. Benchabane, and K. Bekkour, "Rheological characterization of poly(ethylene oxide) solutions of different molecular weights," *J. Colloid. Interf. Sci.*, vol. 336, no. 1, pp. 360–367, Aug. 2009.

[8] M. W. Kim, "Surface activity and property of polyethyleneoxide (PEO) in water," *Colloid. Surface. A*, vol. 128, no. 1, pp. 145–154, Aug. 1997.

[9] B. D. Nikolić, B. Kegl, S. D. Marković, and M. S. Mitrović, "Determining the speed of sound, density and bulk modulus of rapeseed oil, biodiesel and diesel fuel," *Therm. Sci.*, vol. 16, pp. 505–514, 2012.

[10] B. Esteban, J.-R. Riba, G. Baquero, A. Rius, and R. Puig, "Temperature dependence of density and viscosity of vegetable oils," *Biomass Bioenerg.*, vol. 42, Jul. 2012.

[11] B. Esteban, J.-R. Riba, G. Baquero, R. Puig, and A. Rius, "Characterization of the surface tension of vegetable oils to be used as fuel in diesel engines," *Fuel*, vol. 102, pp. 231–238, Dec. 2012.

[12] E. Lampsijärvi, J. Heikkilä, I. Kassamakov, A. Salmi, and E. Hæggström, "Calibrated quantitative stroboscopic schlieren imaging of ultrasound in air," in *2019 IEEE IUS*, Oct. 2019, pp. 1651–1654.

[13] W. Thielicke and R. Sonntag, "Particle image velocimetry for MATLAB: Accuracy and enhanced algorithms in PIVlab," *JORS*, vol. 9, no. 1, May 2021.

[14] A. Haider, S. Haider, and I.-K. Kang, "A comprehensive review summarizing the effect of electrospinning parameters and potential applications of nanofibers in biomedical and biotechnology," *Arab. J. Chem.*, vol. 11, no. 8, pp. 1165–1188, Dec. 2018.